Insect Inspired Self-Righting for Fixed-Wing Drones

Charalampos Vourtsis, *Student Member, IEEE*, Victor Casas Rochel, Francisco Ramirez Serrano, William Stewart, *Member, IEEE*, and Dario Floreano, *Senior Member, IEEE*

***Abstract*—Micro Aerial Vehicles (MAVs) are being used in a wide range of applications such as surveillance, reconnaissance, inspection, and search and rescue. However, due to their size and mission profiles, they are prone to tipping over, jeopardizing their operation. Self-righting is an open challenge for fixed-wing drones since existing research focuses on terrestrial and multicopter flying robots with solutions that increase drag and structural weight. Until now, solutions for winged drones remained largely unexplored. Inspired by beetles, we propose a robust and elegant solution where we retrofit a fixed-wing drone with a set of additional wings akin to beetles shell structured wings called elytra. We show that artificial elytra provide additional lift during flight to mitigate their structural weight while also being able to self-right the MAV when it has been flipped over. We performed simulations along with dynamic and aerodynamic experiments to validate our results.**

***Index Terms*—Biologically-inspired robots, mechanism design, robotics in hazardous fields.**

I. Introduction

OVER the past few years, drones have displayed great potential for operating in difficult environments across a great span of applications and mission profiles [1]. These include being deployed in arduous weather conditions, confined spaces, or areas cluttered with debris. During these missions drones are prone to being tipped over. To takeoff again and continue their mission, robots must be able to self-right. To date, studies on self-righting robots have been limited to terrestrial robots and multi-rotor drones, but have not considered winged aircraft. In this letter we present the first self-righting winged drone.

We accomplished this by taking inspiration from the *coleoptera* order, commonly known as beetles. Beetles have shown a remarkable ability to self-right after falling to the ground by using an outer set of hardened wings called elytra, (singular: elytron) displayed in Fig. 1 (A) [2], [3]. These elytra serve to provide the insect with self-righting capacity as well as producing auxiliary lift during flight. In this way, the added weight and complexity of the second set of wings is offset by the additional lift they produces [4]. Similarly, we incorporated a set of artificial elytra made from a hybrid carbon fiber and Kevlar composite fabric onto a fixed-wing MAV (Fig. 1 (B)). The elytra are attached through two sets of two servos allowing them to be swept back and pitched 180° forward. By first sweeping the wings backwards and then pitching them forward, the aircraft can flip itself over.

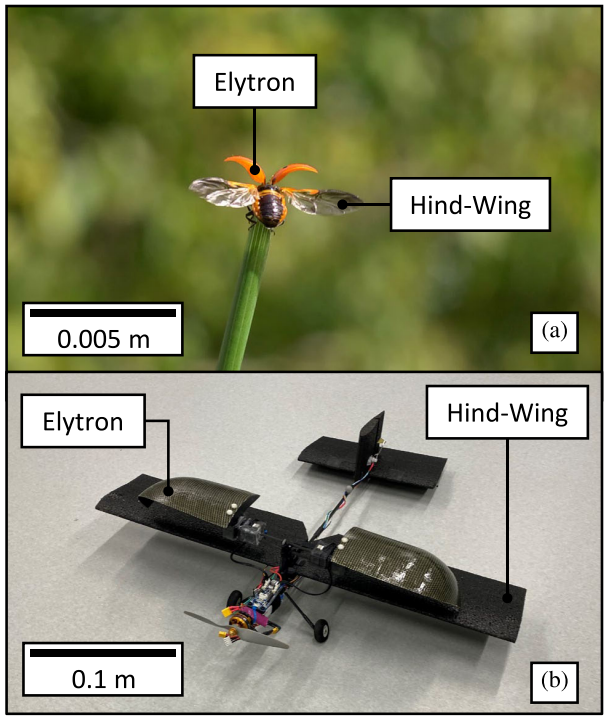

Fig. 1. (A) Ladybug (*Coccinellidae*) with spread wings (Adapted from [5]). Ladybugs, as all flying beetles, have two sets of wings: the hind-wings and the elytra. (B) Ely has a set of fixed-wings akin to the beetle's hind-wings and a set of artificial elytra.

We characterized the performance of the artificial elytra both in terms of self-righting and aerodynamics. Our experiments showed that there is no trade-off in performance between self-righting and aerodynamic efficiency. Namely, larger span elytra produce faster self-righting than shorter span elytra, without an appreciable difference in aerodynamic performance. Further, we demonstrate that a simple biplane model is adequate to predict aerodynamic performance in cruise conditions.

Manuscript received March 1, 2021; accepted June 16, 2021. Date of publication July 9, 2021; date of current version July 23, 2021. This letter was recommended for publication by Associate Editor Y. Peng and Editor X. Liu upon evaluation of the reviewers' comments. This work was supported in part by the European Union's Horizon 2020 Research and Innovation Programme under the Marie Skłodowska-Curie under Grant 754354. It was partially supported in part by the Swiss National Science Foundation through the National Centre of Competence in Research (NCCR), and by the European Union's Horizon 2020 Research and Innovation Programme under Grant 871479 AERIAL-CORE. *(Corresponding author: Charalampos Vourtsis.)*

The authors are with the Laboratory of Intelligent Systems, Ecole Polytechnique Federale de Lausanne, CH1015 Lausanne, Switzerland (e-mail: harry.vourtsis@epfl.ch; victor.casasrochel@epfl.ch; francisco.ramirezserrano@epfl.ch; william.stewart@epfl.ch; dario.floreano@epfl.ch).

This letter has supplementary downloadable material available at https://doi.org/10.1109/LRA.2021.3096159, provided by the authors.

Digital Object Identifier 10.1109/LRA.2021.3096159

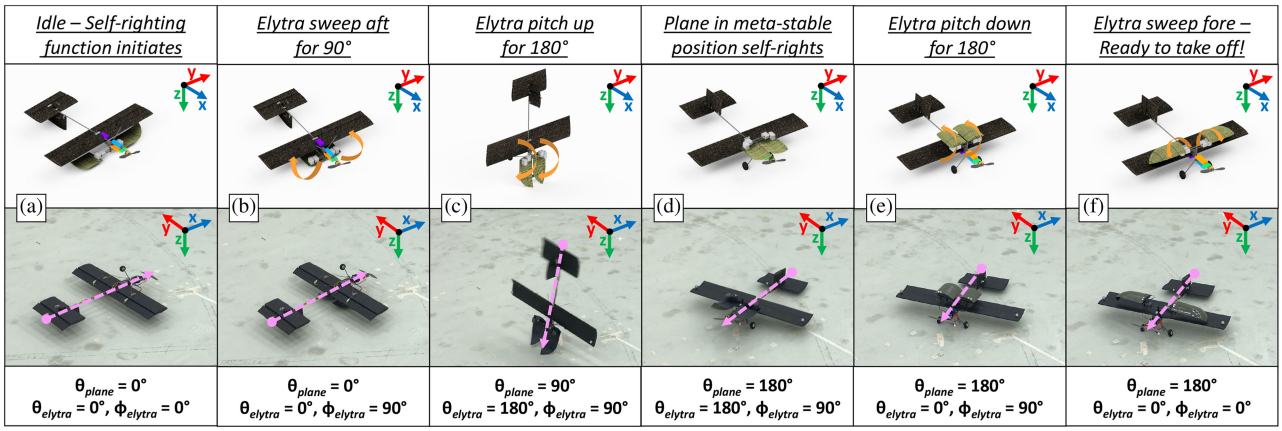

Fig. 2. (A) The self-righting maneuver is triggered as the drone is tipped over. (B), The elytra sweep 90° around their vertical axis. (ϕ_{elytra} from 0° to 90°). (C) Next, the elytra pitch for 180° (θ_{elytra} from 0° to 180°) to rotate the plane around its lateral axis (θ_{plane} from 0° to 180°). (D) The plane is now uprighted. (E) After the uprighting (θ_{plane}=180°), the elytra move back to their flight position (θ_{elytra}=0° ϕ_{elytra}=0°). (F) The plane is ready to take off again with the elytra extended in their initial configuration.

II. Related Work

Self-righting techniques have been extensively investigated both on terrestrial and flying robots. In terrestrial robots, a common strategy is to integrate a separate mechanism that assists with the self-righting. These mechanisms are usually elongated protrusions that use actuators to generate the torque required to self-right the robot [6]–[10]. For example, Casarez and Fearing used a carbon fiber beam to self-right their VelociRoACH robot [11]. In addition to self-righting, Zhang *et al.* added a mass to their beam and were able to re-orient a jumping robot [9]. However, these protrusions and actuators add mechanical complexity and weight. Legged robots have avoided additional weight and complexity by utilizing controllers that allow them to use their legs for self-righting [12], [13]. Some terrestrial robots have used reconfigurable treads or reconfigurable bodies to enable self-righting [14], [15]. Despite their effectiveness, these solutions would require the integration of complex mechanical systems into flying robots, which would increase design and manufacturing complexity as well as energy consumption. Another work explored the principles of cockroaches and used actuated shell structures resembling cockroach wings for self-righting [10], [16]. Despite its effectiveness for self-righting, this strategy also has limitations. The shell configuration in that work would not perform in flight as the chosen self-righting mechanism is not able to extend the wings and generate lift.

Self-righting in flying robots has been limited to integration in multi-copter vehicles. Engineers have utilized multi-actuated protrusions that generate torque to reorient drones into their upright position similar to the ones used on terrestrial robots [17]–[19]. These suffer from performance reduction due to aerodynamic deficiencies and added weight. Prevention of the tipping over of multi-copters was also achieved by combining a caged multi-copter with a gimbal system. After the robot has tipped beyond a given angle, the gimbal assists in reorientation and self-righting [20]. Other researchers optimized the design of the cage, resulting in an ogive shape that allowed passive self-righting when tipped over [21], [22]. However, integrating cages in multi-copters has been found to significantly reduce aerodynamic performance and increase structural weight [23].

Cages, legs, treads, reconfigurable bodies or protrusions would allow fixed-wing drones to self-right, although by substantially decreasing aerodynamic performance, adding weight or increasing mechanical complexity. Our method, inspired from beetles, exploits recent advances in materials and electronics, to allow the integration of an additional set of wings akin to elytra for self-righting while mitigating the performance cost of the added mechanism by generating lift during forward flight.

III. The Self-Righting Operating Principle

In this section, we describe the design principles inspired from the beetles as well as the self-righting performance of a fixed-wing vehicle retrofitted with elytra. Some beetle species utilise their elytra to self-right. In particular, ladybugs, beetles of the family *Coccinellidae* , position their elytra on the ground to stabilize their bodies and self-right using the force generated by their legs or their hind-wings to pitch over their heads [2]. Similar to the animal, we use the drone's elytra to stabilize the fuselage but instead of providing torque using legs, we use actuators connected to the elytra that enable the drone to pitch itself into an unstable position and tip over its nose as presented in Fig. 2. The artificial elytra are installed on a conventional fixed-wing platform code-named Ely. The length of the elytra play a critical role in the self-righting maneuver, as the torque generated on the ground by the elytra, is directly associated with the distance of the applied force.

Beetles feature three degrees of freedom (DOF) in each wing to facilitate flapping and folding in addition to self-righting [2], [24]. Because this study is focused only on self-righting and not on flapping or folding, we use only the required two out of the three DOFs, which keeps weight and structural complexity low. When the self-righting maneuver is triggered (Fig. 2 (A)),

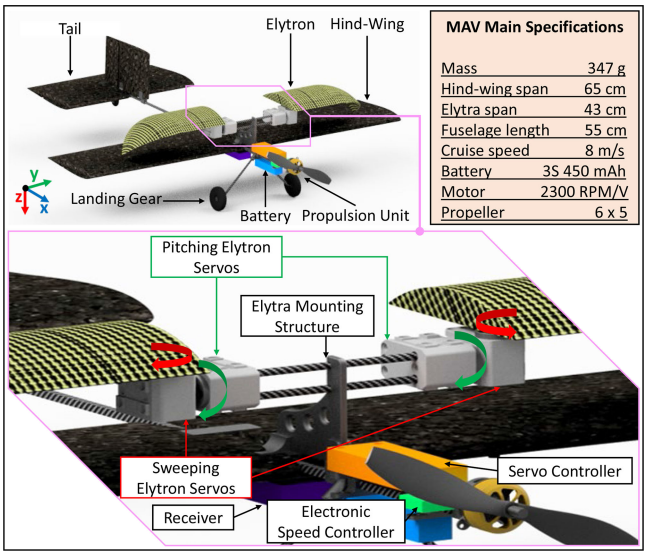

Fig. 3. The winged drone, code-named Ely, with detail of the self-righting mechanism composed of elytra that rotate in pitch and sweep through a pair of servos controlled by an on-board micro-controller. Specifications are summarized in the inset table.

each elytron is swept (DOF 1) 90° around its vertical axis (ϕ_{elytra} from 0° to 90°) by the sweeping servomotor (Fig. 2 (B)). Next, the pitching servomotor pitches (DOF 2) the elytron 180° (θ_{elytra} from 0° to 180°) to rotate the plane about its lateral axis (θ_{plane} from 0° to 180°) (Fig. 2 (C)). After the uprighting (θ_{plane}=180°), the elytra move back to their flight position (θ_{elytra}=0°, ϕ_{elytra}=0°) (Fig. 2 (D - E)). After the self-righting maneuver, the drone is ready to take off again (Fig. 2 (F)).

IV. Ely - the Self-Righting MAV

Ely is a conventional fixed-wing MAV with a single electric motor in tractor configuration (Fig. 3). The hind-wings were made from Expanded Poly Propylene (EPP); a resilient and highly flexible foam material. The elytra were 3D printed with Acrylonitrile Butadiene Styrene (ABS) plastic and were re-enforced with carbon-Kevlar composite fabric and epoxy adhesive for added resilience. The fuselage was fabricated from a carbon fiber rectangular beam and the hind-wings and elytra were attached with 3D printed ABS mounts. We used a low Reynolds number airfoil for Ely's hind-wings, namely Eppler E168. The elytron geometry was modeled with a simplified ogive shell representation where the main dimensions were obtained by scaling up those of the insect. For the hind-wings and the elytra, the spans and chords were respectively scaled so as to correspond to standard Micro Aerial Vehicle wing proportions [25].

The vertical separation distance between the hind-wings and elytra was optimised in computer-aided design (CAD) for reducing structural weight. On a beetle, the elytra are positioned forward of the hind-wings (positive stagger), as both pairs of wings require space for flapping. On Ely, the thrust is generated by the propeller and the wings are fixed; therefore, for simplicity, the hind-wings and elytra are aligned at the quarter chord (aerodynamic center).

V. Self-Righting Elytra - Mechanical Characterization

A. Simulation of the Self-Righting

To validate the self-righting principle, and characterize design parameters such as the amplitude of the sweeping and pitching motions, a simulation of the self-righting maneuver was developed. The simulator was built using Simscape Multibody in a Simulink environment [26]. Simscape simulates interactions between multiple bodies for 3D mechanical systems.

The Simscape model includes two solid bodies for the elytra, two for the sweeping servos, one for the propeller and one body for the rest of the plane (including the pitching servos). Finally, a spatial contact force block connects each solid block of the aircraft to the ground to simulate their interaction. In our model (Fig. 4), each elytron is connected to the sweeping servo by the yaw revolute joint, which models the sweeping motion. That servo is connected to the aircraft solid body by the pitch revolute joint which models the pitching of the elytra. Since the propeller is in contact with the ground while self-righting and is free to rotate, the propeller solid body is connected to the aircraft solid body by the propeller revolute joint.

In each solid block (except the ground which is fixed), the mass, the position of the Center of Gravity (COG), and the moments and products of inertia are specified. These values were taken from the CAD model of Ely. Each revolute joint requires a torque, a damping factor and a spring stiffness factor. These factors characterize the behaviour of the revolute joint and they are set to match their respective components on Ely. The simulation begins with the elytra already swept back, so torque values were only applied to the revolute joints responsible for pitching the elytra on the ground. This joint is additionally bounded with an upper and lower limit on rotation so that the elytra do not exceed 180° of rotation during self-righting. Similarly to the revolute joints, there are factors to characterize the spatial contact force between the aircraft and the ground. The static and dynamic friction coefficients were measured on Ely. Each parameter of the spatial contact force and revolute joint blocks are given in the Supplementary Material - Supplementary_Table.

The self-righting simulation assumes that the solid bodies such as the elytra and fuselage are perfectly rigid, and hence neglects aerodynamic effects and deformations during the self-righting maneuver. Two different torques (0.31 and 0.39 Nm) and three different elytron lengths (11, 14, and 17 cm) were simulated. The simulations showed that for the elytron measuring 11 cm, the aircraft was not able to self-right, regardless of the torque (Fig. 5 (B)). The simulations of the plane equipped with 14 cm elytra was capable of self-righting only when the highest torque was applied. Finally, the simulations of 17 cm long elytra were successful at self-righting no matter the torque. These simulations indicate that larger elytron lengths have better self-righting performance. The simulations were also used to predict the time required for the robot to self-right. They indicated that when successful, the vehicle could right itself in less than a second, but that there was some variation with elytron length. That is, longer elytra will self-right the vehicle faster than shorter elytra.

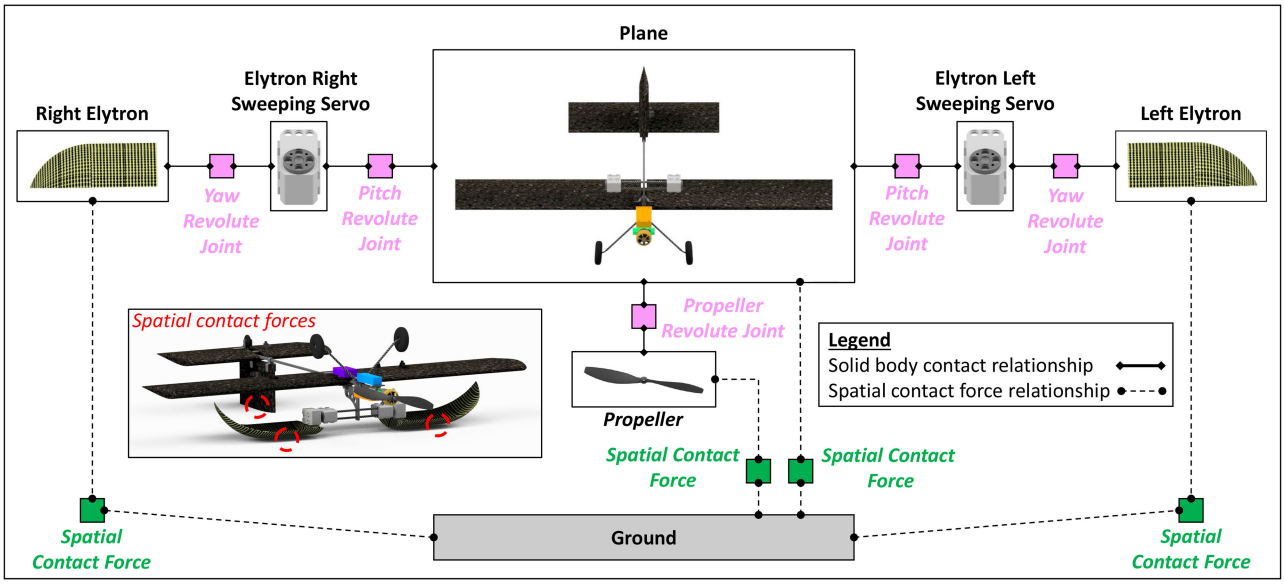

Fig. 4. The simplified Simulink - Simscape model of Ely highlights the main blocks (solid body, 1 DOF revolute joint, spatial contact force) and their relationships.

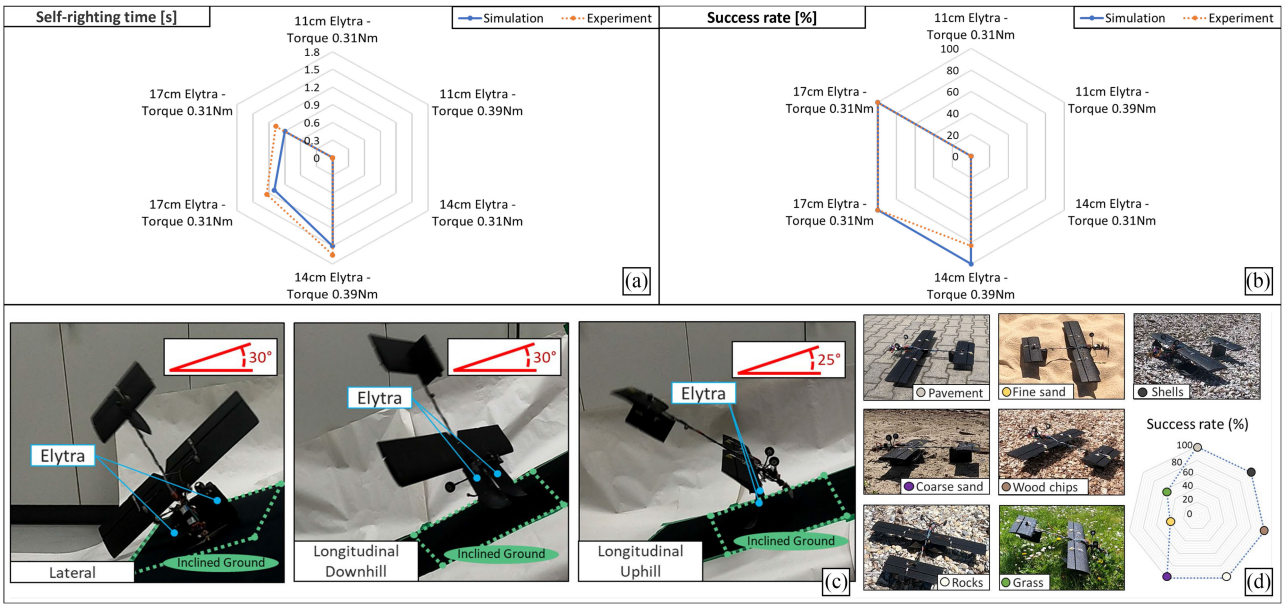

Fig. 5. (A) Simulated and experimentally measure self-righting time. (B) Simulated and experimentally measure self-righting success. (C) Experimental robustness validation of the mechanism in inclined terrain of lateral vehicle position of 30° to −30°, longitudinal downhill of 0° to 30° and longitudinal uphill of 0° to 25°. (D) Experimental robustness validation of the mechanism in seven types of uneven terrain.

To have a better understanding of why longer elytra are more successful at self-righting, we split the self-righting maneuver into two phases. The rising phase takes place when θ_{plane} is between 0° to 90° (Fig. 2 from (B) to (C)) and the falling phase happens from 90° to 180° (Fig. 2 from (C) to (D)). If the COG passes through 90° (Fig. 2 (C)), then the force of gravity will cause the plane to fall. Once the elytra have completed their 180° pitch rotation, they cannot contribute to rotating the plane anymore. If the elytra are long enough that the COG has reached 90° before the elytra have completed their 180° rotation, then the plane is guaranteed to transition to the falling phase. Therefore, with elytra length at or beyond the specific elytron length (Fig. 6), the only factor determining if the plane can self-right is whether there is enough torque to lift the COG up to 90° or not. In our case, the simulations of the 17 cm elytra correspond to this scenario, as the specific elytron length of Ely is 16 cm. Conversely, elytra shorter than the specific elytron length will finish their pitching revolution within the rising phase. This will result in one of two different scenarios. The first scenario is if the torque is high enough that when the elytra reach 180°, the plane has enough momentum to reach the falling phase. Consequently, the first scenario implies that the self-righting maneuver is successful. This corresponds to the simulations of 14 cm elytra and a torque of 0.39 Nm. The second scenario is if

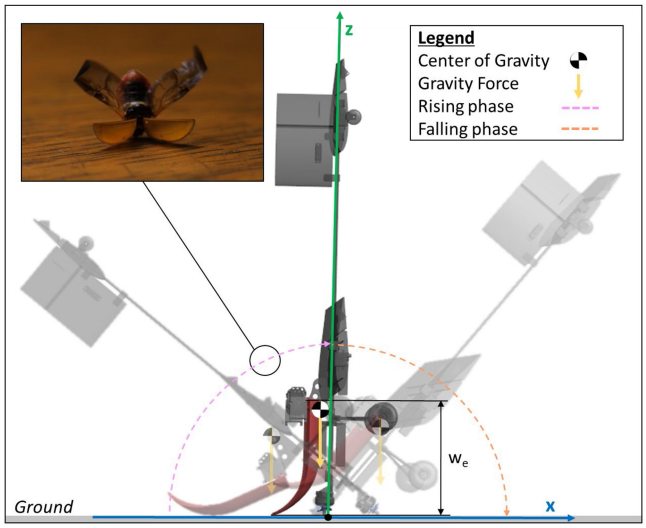

Fig. 6. Specific Elytron length that pushes on the ground during the entire rising phase and completes its pitching revolution (θ_{elytra}=180°) at the moment the plane enters in the falling phase ((θ_{plane}=90°)). The specific elytron length corresponds to the distance between the nose of the aircraft and the point of rotation of the elytron. Insect picture adapted from [27].

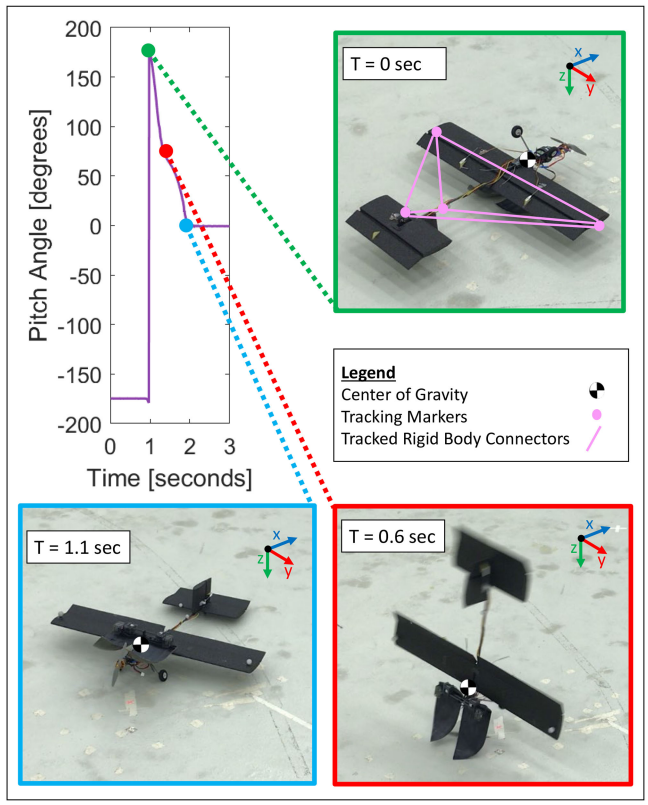

Fig. 7. Sample of the experimental self-righting characterization. A motion capture system was used to record the motion during the self-righting process in real time. Five passive tracking markers were attached to the plane and tracked in the 3D space. Pitching angle and self-righting time was characterized for different elytra configurations and torques. The graph shows a sample diagram for the configuration of the vehicle with the 17 cm elytra and 0.39 Nm.

the torque is not high enough to generate enough momentum to carry the plane to the falling phase, resulting in an unsuccessful self-righting maneuver. This also corresponds to the case of 14 cm elytra, but this time at a torque of 0.31 Nm.

B. Experimental Validation of Self-Righting Simulation

To validate the results of the simulation, experiments were conducted which consisted of the airplane attempting the self-righting maneuver for each of the configurations simulated, namely, three different elytron lengths (11, 14, 17 cm) and two different torques (0.31 and 0.39 Nm). For each configuration (Elytron length - torque), the experiments were repeated four times. The experiments took place in an Optitrack motion capture hall. Five tracking markers were glued to specific locations (Fig. 7) on the plane. In the motion capture system's software, these markers comprised a rigid body, whose motion was recorded during the self-righting maneuver.

The self-righting success rates and times in simulations and experiments are shown in Fig. 5 (A), (B). The results of the experiments were found by computing the mean of the trials for each configuration. The experiments showed that when the plane is equipped with short elytra (measuring 11 cm in span), it cannot self-right (0 % success) no matter the torque. This matches the results from the simulations. The medium elytra (14 cm) were also not able to self-right when using the lowest tested torque and were 83% successful with higher torque (0.39 Nm), closely matching the simulation which predicted 100% success for this case. Finally, the elytra measuring 17 cm were 100% successful regardless of the torque, which also matched the simulation results.

In Fig. 5 (A), for the same elytron length and torque, the simulation shows a maximum of 10% difference in self-righting time compared with the experiments. This indicates good agreement between the simulation and physical vehicle.

These experiments have characterized the self-righting performance on flat and even terrain. However, in many applications, the robot will be required to self-right on more rugged terrain. We therefore conducted a validation of the self-righting mechanism on seven different terrain as well as inclined ground (Fig. 5 (C) and (D)). For this experiment, the 17 cm elytra were used with 0.31 Nm torque. For each ground type and inclination, the self-righting maneuver was conducted five times. The inclinations tested were 10°, 20°, and 30°. Above 30°, the vehicle could no longer self-right at all because the vehicle would slide down the inclination. For each inclination angle, we tested three different vehicle orientations, longitudinal uphill, longitudinal downhill, and lateral. With only one exception, we found that the vehicle self-rights with a 100% success rate for each tested inclination angle in all headings. The exception was longitudinal uphill, which was not able to self-right at 30°, so for this case we also tested 25°, at which inclination it achieved a 100% success rate. The mechanism was also tested on flat ground, but with varying terrain types. In these tests, the mechanism displayed a 100% self-righting success in five out of the seven tested terrains and thus enabling self-righting for vehicles with versatile range

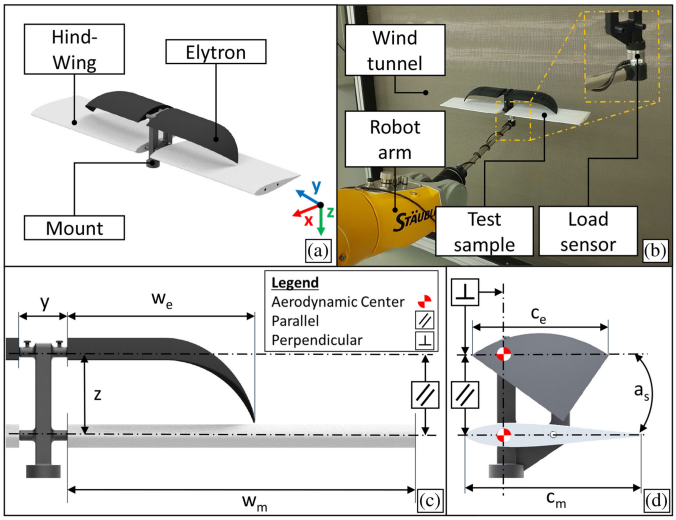

Fig. 8. (A) Isometric view of the test sample showing main features. (B) Experimental setup composed of the aerodynamic test article, Stäubli robot arm, WindShape wind tunnel and ATI Nano25 F/T Sensor. In this figure the test article is composed of a mount, hind-wings and elytra of 17 cm wingspan. (C) Front view of the test article (D) Side view of the test article.

of operational environments. The two terrains which did not have a 100% success rate were in grass and fine sand.

VI. Self-Righting Elytra - Aerodynamic Characterization

An aerodynamic test article was built to investigate the aerodynamic properties of the proposed self-righting mechanism (Fig. 8), namely the lift and drag coefficients as well as the lift-to-drag ratios of the dual-wing system as compared with a mono-wing system. The test article consists of a central wing mount with bonded hind-wings and slots for swapping elytra in and out (Fig. 8(A)). Each elytron is equipped with two carbon fiber rods that slide into the mount slots. Set screws were used to prevent the elytra from slipping in the spanwise direction (Fig. 8(C-D)). A 6 DOF ATI Nano25 loadcell was mounted to the base of the test article at its aerodynamic center. Through combinations of different elytra, seven test article configurations were aerodynamically tested. These configurations were the three different elytra lengths corresponding to the lengths characterized for self-righting with hind-wings, those same three elytra without hind-wings, and the hind-wings without elytra (Fig. 9).

The test article was attached to a Stäubli robotic arm, which in turn was placed in an open-jet WindShape wind tunnel [28] (Fig. 8 (B)). The robot was programmed to set the test article at a commanded angle of attack. Throughout the experiments, the angle of attack range was varied between -4° and 17° in increments of 3°. The uncertainty in angle of attack was estimated to be $< 0.2^\circ$. To ensure the air flow was smooth, the test sample was positioned such that the leading-edge of the hind-wings was 18 cm from the wind tunnel filter. Tests were run at a wind speed of 8.3 m/s which corresponds to a Reynolds number of about 68 000. At each angle of attack, 500 data samples were recorded at 100 Hz after waiting a few seconds to let the wings reach steady-state. The measured forces were then projected to obtain lift and drag measurements, from which lift and drag coefficients can be calculated.

A. Aerodynamic Experimental Results

Fig. 9 shows that elytra generate non-negligible lift which mitigates the weight penalty they incur from an angle of attack of 2° to 17° (Fig. 9 (C)). For angles of attack from -4° to about 6°, the elytra hind-wings system, increases the aerodynamic efficiency by displaying a higher lift-to-drag ratio than that of hind-wings (Fig. 9 (B)). At higher angles of attack the performance of the elytra and hind-wings system deteriorates due to the elytra hind-wings aerodynamic interactions. However, for most UAV applications, this is a minor effect as wing systems usually fly at angles of attack between 2° and 5°. The additional lift production is the reason that elytra as self-righting mechanisms outperform other systems in the state of the art. Self-righting systems with similar weight, such as gimbal-cages, legs or elongated protrusion mechanisms, show approximately a consistent 70% higher drag without having the lift generation benefits of the elytra [23], [29] (Fig. 9 (B)). There is no consistent trend between elytra of different lengths (Fig. 9 (B)). For instance, below an angle of attack of about 3° the shortest elytra have the highest lift coefficient, but above 3°, the longest elytra have the highest lift coefficient (Fig. 9 (B)).

To estimate the aerodynamic effects of the elytra on the hind-wings, we applied the biplane model. Fig. 9 (A) displays the aerodynamic performance of the hind-wing and elytra system alongside the predictions from the biplane model. The total lift coefficient for a biplane can be defined as [30]:

$$C_{L_{total}} = \frac{A_{HW} C_{L_{HW}} + A_E C_{L_E}}{A_{HW} + A_E} \tag{1}$$

$$C_{D_{total}} = \frac{A_{HW} C_{D_{HW}} + A_E C_{D_E}}{A_{HW} + A_E} \tag{2}$$

Where $C_{L_{total}}$ and $C_{D_{total}}$ are the total lift and drag coefficients based on total planform area $(A_{HW} + A_E)$. A_{HW}, A_E are the Hind-wing and Elytra wing areas respectively, and $C_{L_{HW}}$, C_{L_E}, $C_{D_{HW}}$, C_{D_E} are respectively, the independent lift and drag coefficients of the hind-wings and elytra. Fig. 9 (A) presents the measured lift-to-drag ratios of the hind-wing and elytra of different spans as well as the lift-to-drag predicted by the biplane model. The biplane model is able to most accurately predict the measurements for small angles of attack, with the highest precision being achieved at 5° for the 14 and 17 cm elytra and at 8° for the 11 cm elytra. This corresponds closely to Ely's cruise angle of attack of about 5°. Differences between measurements and the biplane model are likely due to interactions between the elytra wing tips and airflow over the upper surface of the hind-wings.

While short elytra achieve the highest aerodynamic performance at cruising angles, they are unable to self-right with the selected motors. At the cruise angle of attack of about 5°, all

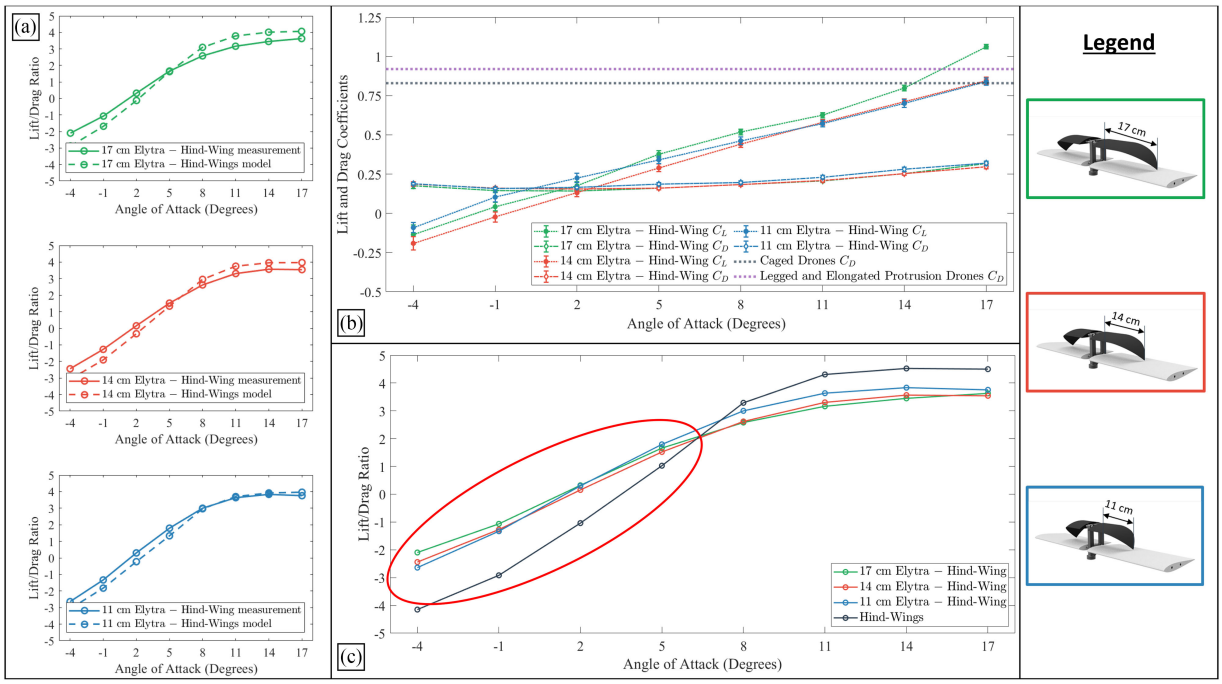

Fig. 9. Aerodynamic characterization of hind-wings with different elytra configurations. (A) Lift/Drag ratio for the aerodynamic test sample mounted with hind-wings and different elytra lengths in comparison with their theoretical model. (B) Lift and drag coefficients of the test sample mounted with elytra of different lengths and in comparison with existing self-righting solutions in the state of the art. (C) Lift/Drag ratio of the hind-wings and of hind-wings with different elytra configurations.

Fig. 10. Image from the flight experiments of Ely.

three elytra lengths perform similarly. Thus, the selection of elytra lengths for Ely should be 17 cm as they achieved a 100% self-righting success rate. Alternative design objectives, such as increased compactness could favor shorter span elytra, in cases such as this, a trade-off is made with self-rightability over aerodynamic performance.

VII. Free Flight Test

The flight tests consisted of first dropping Ely onto the ground such that it landed in an inverted position. At impact, the elytra absorbed the landing loads and immobilized the drone. Then, the self-righting function was manually triggered. The pre-programmed self-righting function autonomously began after 5 seconds. As described in previous sections, the elytra are first swept back 90° and then pitched forward 180° to flip the plane into its upright position. After uprighting, the elytra move back to their flight position. Next the pilot engages full throttle and the plane takes off. Ely flew steadily at an approximate speed of 8 m/s (Fig. 10). The flight test was carried out in calm wind conditions of less than 2 km/h. The plane successfully flew for 45 seconds before landing in short grass. The flight test can be viewed in Supplementary Material - Supplementary_Video.

VIII. Conclusion

In this letter, we present an insect inspired, self-righting solution for small winged drones. We integrated a set of artificial elytra that are utilised for self-righting as well as providing additional lift, mitigating the extra energy use incurred by the self-righting mechanism. We characterized the self-righting capabilities and the aerodynamic performance of a flight worthy drone and studied the trade-off between self-righting mechanics and aerodynamic performance.

The proposed solution is suitable for fixed-wing drones at the Micro Aerial Vehicle scale [25]. In this study, we used widely available materials. Elytra materials with different mechanical properties could be used to enable self-righting in a variety of challenging environments with diverse surface composition in terms of temperature, humidity and friction coefficients. Elytra geometries with differing levels of camber or airfoil shapes

could be employed depending on the aerodynamic performance required. Moreover, the simple yet robust mechanical design of the self-righting mechanism makes the system fit for use not only in aerial vehicles, but also in terrestrial and marine robots that require self-righting capabilities.

REFERENCES

[1] D. Floreano and R. J. Wood, "Science, technology and the future of small autonomous drones," *Nature*, vol. 521, no. 7553, pp. 460–466, May 2015.

[2] L. Frantsevich, "*Righting kinematics beetles (Insecta: Coleoptera)*," Arthropod Structure & Development, vol. 33, no. 3, pp. 221–235, Jul. 2004.

[3] J. Zhang, J. Li, C. Li, Z. Wu, H. Liang, and J. Wu, "Self-righting physiology of the ladybird beetle coccinella septempunctata on surfaces with variable roughness," *J. Insect Physiol.*, vol. 130, no. 104202, pp. 1–9, Feb. 2021, Art. no. 104202.

[4] L. C. Johansson, S. Engel, E. Baird, M. Dacke, F. T. Muijres, and A. Hedenström, "Elytra boost lift, but reduce aerodynamic efficiency in flying beetles," *J. Roy. Soc. Interface*, vol. 9, no. 75, pp. 2745–2748, Oct. 2012.

[5] wildwatertv, "Ladybird taking off from a grass stalk." [Online]. Available: https://www.pond5.com/stock-footage/item/8658289-ladybird-taking-grass-stalk-slow-motion

[6] M. I. Wallace, J. F. Burn, R. A. Hyde, C. Melhuish, and T. Pipe, "Biologically Inspired Solutions for Compliant Limb UGVs," in 2nd SEAS DTC Technical Conf., pp. 1–9, 2007.

[7] C. C. Kessens, D. C. Smith, and P. R. Osteen, "A framework for autonomous self-righting of a generic robot on sloped planar surfaces," in *Proc. IEEE Int. Conf. Robot. Automat.*, 2012, pp. 4724–4729.

[8] H. Tsukagoshi, M. Sasaki, A. Kitagawa, and T. Tanaka, "Design of a higher jumping rescue robot with the optimized pneumatic drive," in *Proc. IEEE Int. Conf. Robot. Automat.*, 2005, pp. 1276–1283.

[9] J. Zhang, G. Song, Z. Li, G. Qiao, H. Sun, and A. Song, "Self-righting, steering and takeoff angle adjusting for a jumping robot," in *Proc. IEEE/RSJ Int. Conf. Intell. Robots Syst.*, 2012, pp. 2089–2094.

[10] Q. Xuan and C. Li, "Randomness in appendage coordination facilitates strenuous ground self-righting," *Bioinspiration Biomimetics*, IOP Publishing United Kingdom, vol. 15, pp. 1–14, no. 6, Oct. 2020, Art. no. 065004

[11] C. S. Casarez and R. S. Fearing, "Dynamic terrestrial self-righting with a minimal tail," in *Proc. IEEE/RSJ Int. Conf. Intell. Robots Syst.*, 2017, pp. 314–321.

[12] U. Saranli, A. A. Rizzi, and D. E. Koditschek, "Model-based dynamic self-righting maneuvers for a hexapedal robot," *Int. J. Robot. Res.*, vol. 23, no. 9, pp. 903–918, Sep. 2004.

[13] S. Peng, X. Ding, F. Yang, and K. Xu, "Motion planning and implementation for the self-recovery of an overturned multi-legged robot," *Robotica*, Cambridge University Press, United Kingdom, vol. 35, no. 5, pp. 1107–1120, 2017, edition: 2015/12/23 Publisher: Cambridge University Press.

[14] H. Schempf *et al.*, "Pandora: Autonomous urban robotic reconnaissance system," in *Proc. IEEE Int. Conf. Robot. Automat.*, May 1999, vol. 3, pp. 2315–2321.

[15] Z. Guanghua, D. Zhicheng, and W. Wei, "Realization of a modular reconfigurable robot for rough terrain," in *Proc. Int. Conf. Mechatronics Automat.*, 2006, pp. 289–294.

[16] C. Li, C. C. Kessens, R. S. Fearing, and R. J. Full, "Mechanical principles of dynamic terrestrial self-righting using wings," *Adv. Robot.*, vol. 31, no. 17, pp. 881–900, Sep.. 2017.

[17] A. Briod, A. Klaptocz, J. Zufferey, and D. Floreano, "The AirBurr: A flying robot that can exploit collisions," in *Proc. ICME Int. Conf. Complex Med. Eng.*, 2012, pp. 569–574.

[18] A. Klaptocz, L. Daler, A. Briod, J.-C. Zufferey, and D. Floreano, "An active uprighting mechanism for flying robots," IEEE Trans. Robot., vol. 28, no. 5, pp. 1152–1157, Oct. 2012.

[19] A. Kossett and N. Papanikolopoulos, "A robust miniature robot design for land/air hybrid locomotion," in *Proc. IEEE Int. Conf. Robot. Automat.*, 2011, pp. 4595–4600.

[20] A. Briod, P. Kornatowski, J.-C. Zufferey, and D. Floreano, "A collision-resilient flying robot," *J. Field Robot.*, vol. 31, no. 4, pp. 496–509, 2014.

[21] M. Kovač, M. Schlegel, J.-C. Zufferey, and D. Floreano, "Steerable miniature jumping robot," *Auton. Robots*, vol. 28, no. 3, pp. 295–306, Apr. 2010.

[22] E. Beyer and M. Costello, "Performance of a Hopping Rotochute," *Int. J. Micro Air Veh.*, Sage Publications, USA, vol. 1, no. 2, pp. 121–137, Jun. 2009

[23] P. Kornatowski, S. Mintchev, and D. Floreano, "An origami-inspired cargo drone," in *Proc. IEEE/RSJ Int. Conf. Intell. Robots Syst.*, 2017, pp. 6855–6862

[24] L. Frantsevich, "Geometry of elytra opening and closing in some beetles (coleoptera, polyphaga)," *J. Exp. Biol.*, vol. 208, no. 16, pp. 3145–3158, Aug. 2005.

[25] M. Hassanalian and A. Abdelkefi, "Classifications, applications, and design challenges of drones: A review," *Prog. Aerosp. Sci.*, vol. 91, pp. 99–131, May 2017.

[26] "Simulink - Simulation and Model-Based Design," [Online]. Available: https://www.mathworks.com/products/simulink.html

[27] vexedart, "Tiny but Powerful Little Bug Getting up From Being Stuck on Its Back. Lady Bug O." [Online]. Available: https://www.pond5.com/

[28] "WindShape - Drone Test Equipment and Services - Wind Tunnel," [Online]. Available: https://www.windshape.ch/

[29] C. J. Salaan, Y. Okada, K. Hozumi, K. Ohno, and S. Tadokoro, "Improvement of UAV's flight performance by reducing the drag force of spherical shell," in *Proc. IEEE/RSJ Int. Conf. Intell. Robots Syst.*, 2016, pp. 1708–1714.

[30] R. Jones, D. J. Cleaver, and I. Gursul, "Aerodynamics of biplane and tandem wings at low reynolds numbers," *Experiments Fluids*, vol. 56, no. 6, pp. 1–25, Jun. 2015.